Calibrated, Multiband Optical Emissions from Rocket-Triggered Lightning

Mason G. Quick[1*], E. Philip Krider[1], Martin A. Uman[2], Douglas M. Jordan[2], Jonathan D. Hill[3], William R. Gamerota[2]

1. University of Arizona, Tucson, Arizona, United States of America
2. University of Florida, Gainesville, Florida, United States of America
3. Stinger Ghaffarian Technologies, Kennedy Space Center, Florida, United States of America

ABSTRACT:

Broadband radiometric measurements of the optical emissions from a 62 m section of rocket-triggered lightning (RTL) channels have been made at ultraviolet (UV), visible and near infrared (VNIR), and long-wave infrared (LWIR) wavelengths. The signals were recorded from a distance of 198 m at the University of Florida International Center for Lightning Research and Testing (ICLRT) during the summer of 2012. The UV radiometer measured wavelengths from 200 to 360 nm, the VNIR radiometer measured from 400 to 1000 nm, and a LWIR sensor, together with an 8 to 12 µm passband filter, covered from 8 to 12 µm. The ICLRT provided time-correlated measurements of current at the base of the channels. Following the onset of a return stroke, the dominant mechanism for the initial rise of the UV and VNIR waveforms was the geometrical growth of the channel in the field-of-view of the sensors. The UV emissions peak about 0.7 µs after the current peak, and the average peak spectral power emitted at the source per unit length of channel was 10 ± 7 kW/(nm-m) in the UV. The VNIR emissions peaked 0.9 µs after the current peak, and the VNIR spectral power peaked at 7 ± 4 kW/(nm-m). The LWIR emissions peaked 30 to 50 µs after the current peak, and the mean peak spectral power was 940 ± 380 mW/(nm-m), a value that is about 4 orders of magnitude lower than the other spectral emissions. Examples of the optical waveforms in each spectral band will be shown as a function of time and will be discussed in the context of the current measured at the channel base.

∗ Contact information: Mason G. Quick, Institute of Atmospheric Physics, University of Arizona, Physics-Atmospheric Sciences Bldg., Rm 542, 1118 E 4th St., PO Box 210081, Tucson, Arizona 85721-0081, United States of America. Email: MGQuick@atmo.arizona.edu

INTRODUCTION

Broadband optical signatures have been used for many years to study lightning processes such as leaders, return strokes (RS), continuing currents, M-components, etc. in rocket-triggered lightning (RTL) [*Jordan et. al* 1992; *Idone and Orville* 1985; *Mach and Rust* 1989; *Wang et. al* 1999a, 1999b, 2005, 2013, 2014; *Chen et. al* 2003, *Olsen et. al* 2004; *Qie et. al* 2011; *Quick and Krider* 2013; *Winn et. al* 2012; and others]. Nearly all of these studies have been limited to emissions in the visible and near infrared (VNIR) spectral bands and few have been calibrated.   *Guo and Krider* [1982, 1983] and *Quick and Krider* [2013] reported calibrated measurements of the VNIR emissions from return strokes in natural lightning, and here we will present the first calibrated measurements of the optical emissions from return strokes in RTL. The radiometers covered three broad spectral bands: the ultraviolet (UV, 200-360 nm), the VNIR (400-1000 nm), and the long wave or "thermal" infrared (LWIR, 8-12 µm).

All measurements were made during the summer of 2012 at the International Center for Lightning Research and Testing (ICLRT) at Camp Blanding, Florida, as part of a collaborative study sponsored by DARPA through the University of Florida (see for example: *Hill et. al* 2012, 2013, *Schaal et. al* 2012, *Gamerota et. al* 2013, *Pilkey et. al* 2013). The optical irradiances [W/m^2] in each spectral band were measured at a distance of 198 m from the ground-launcher and were time-correlated with currents measured at the channel base to a precision of 0.1 µs.   We will begin by describing the sensors and the measurement system, and then we will give examples of the optical waveforms in each spectral band. Next, we describe our estimates of the spectral power that was emitted by the source, and finally we will discuss the results.

EXPERIMENT

A suite of three radiometers that viewed the same vertical section of RTL channels was used to make all optical measurements.   Each radiometer contained a single element photoelectric detector in combination with a filter, and had a field of view (FOV) that was geometrically limited by a set of optical baffles to about 17 degrees in the vertical and 45 degrees in the horizontal. The RTL channel segment that was measured was between 10 and 72 m above ground. The geometry of the observations is shown schematically in Fig. 1, and the measured (vertical) angular response of the radiometers is shown in Fig. 2. The sensor electronics were AC coupled, using a time constant of about 1 second, but had varying bandwidths as described below. All signals were recorded on a Yokogawa [Model DL750] 8-channel digital storage oscilloscope (DSO) that sampled at a frequency of 10 MHz using 12-bit A/D converters on each channel. The input modules on the DSO had a cutoff frequency of 3 MHz to avoid aliasing.

 The UV radiometer consisted of a SiC photodiode that responded to UV wavelengths, and the amplifying electronics had a bandwidth of 3 MHz. The VNIR radiometer used a silicon PIN photodiode in conjunction with a blue filter to obtain a nearly flat spectral response over the VNIR band, and the electronics also had a bandwidth of 3 MHz. The measured spectral response of the UV and VNIR radiometers are shown in Fig. 3. The LWIR radiometer consisted of a HgCdTe photoconductor with an 8-12 µm passband filter that limited the sensor response to an atmospheric window in the LWIR. The sensor was housed in a Dewar flask and cooled to liquid nitrogen temperatures to reduce thermal noise. The spectral responsivity of the LWIR radiometer peaked at about 11 µm, as shown in Fig. 4, but the bandwidth of the electronics was limited to 500 kHz because of the high gain required in this spectral range.
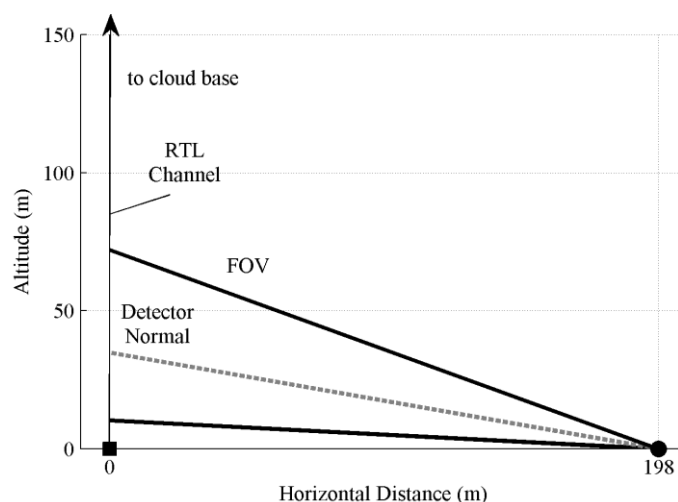
Figure 1: Scale drawing of the viewing geometry for all 3 radiometers. The vertical line shows an ideal RTL channel between the ground launcher and the cloud base. The horizontal distance, *D*, between the optical radiometers and the launcher was 198 m. The vertical FOV shown here corresponds to the 20% level of the angular response curve shown in Fig. 2. A ray at normal incidence to the detector has been included to illustrate the sensor elevation angle. All radiometers used an elevation angle of 10 degrees and viewed a vertical channel segment between altitudes of 10 and 72 m.
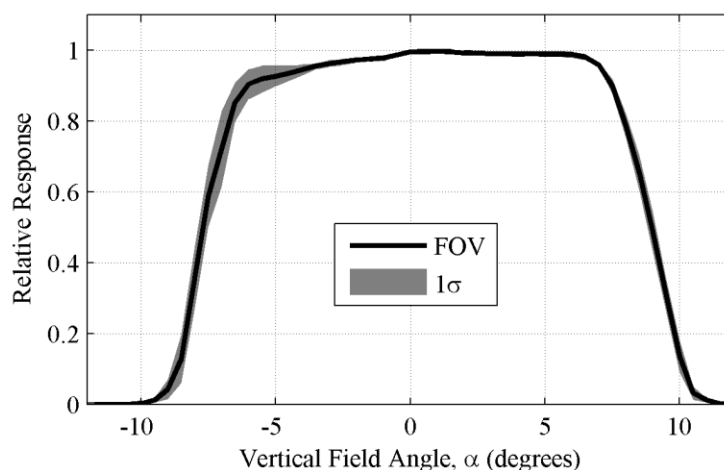

Figure 2: Measured angular response of all radiometers as a function of the field angle, α.
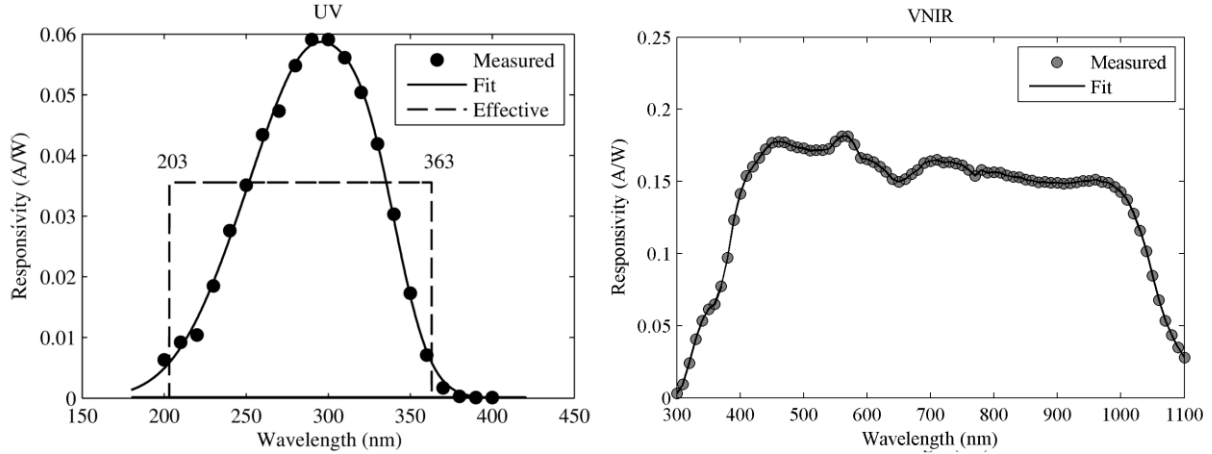
Figure 3:   Left: Spectral response of the UV radiometer.   Because the response is not flat over the spectral band, a characteristic or "effective" response (dotted line) has been assumed for this radiometer.   Right: Spectral response of the VNIR radiometer.
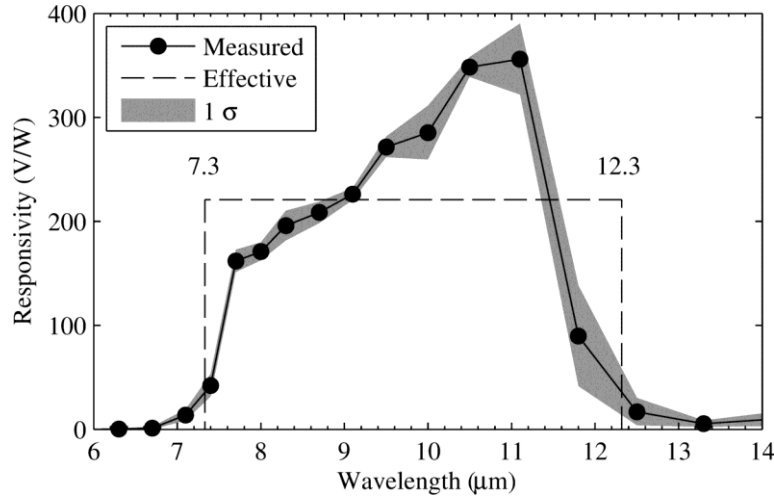

Figure 4:   Spectral response of the LWIR detector and 8-12 μm filter.   Because the response is not flat over this spectral band, a characteristic or "effective" response (dotted line) has been assumed for this radiometer.

METHODS

In order to compare the optical powers that are radiated in each spectral band, we must first normalize the measured irradiance values by the spectral bandwidth (SBW) of the radiometers; we will call the result the *average spectral irradiance*, $\overline{L_\lambda}$, a quantity that has units of [W/m^2-nm].   Given the measured $\overline{L_\lambda}$ waveforms, two independent estimates of the average source power per unit length of channel can be obtained. The first method is essentially the same as that described in *Guo and Krider* [1983] and *Quick and Krider* [2013] and uses the maximum initial slope of the optical waveform to estimate a time- and space-

average peak power per unit length (designated ℓ_o in previous reports).   This method assumes that the RS channel is an isotropic radiator and that the optical power is approximately constant with height behind an upward propagating front during the onset of the stroke. In this case, the initial slope of the optical signal ($d\overline{L_\lambda}/dt$) will be entirely due to the geometrical growth of the luminous channel in the FOV.   At early times, the stroke is relatively short and can be approximated as straight and vertical.   Therefore if the RS velocity, v, is assumed to be constant with height (1.2×10^8 m/s [*Wang et. al* 2013; *Cummins and Murphy* 2009]) then the average peak spectral power per unit length, $\ell_{\lambda,o}$, can be estimated using the following equation:

$$\ell_{\lambda,o} = \frac{4\pi R^2}{v \cos\alpha} \frac{d\overline{L_\lambda}}{dt} \tag{1}$$

where R is the distance to the source and α is the field angle of the source in the vertical field of the sensor (corresponding to the horizontal axis in Fig. 2).   [Note that we have made an additional correction for the viewing geometry by dividing by cos α.]

The second method takes advantage of the close proximity of the optical sensors to the RTL at the ICLRT.   Specifically, because both the distance to the source and the viewing angle are known, the actual slant range between the channel and radiometers can be determined as a function of height, assuming the channel is straight and vertical and completely fills the vertical FOV.   If the horizontal distance between the source and sensor is D, then a spatial average of the peak spectral power per unit length of channel ($\ell_{\lambda,\mathcal{R}}$) can determined be radiometrically using the following equation.

$$\ell_{\lambda,\mathcal{R}} = \frac{4\pi D}{\sin|\alpha_T| + \sin|\alpha_B|} \overline{L_{\lambda,pk}} \tag{2}$$

Here $\overline{L_{\lambda,pk}}$ is the peak of the average spectral irradiance at the radiometer and α_T and α_B are the upper (top) and lower (bottom) field angles in the FOV.   This approximation also assumes that each channel segment radiates isotropically.

RESULTS

In order to compare the optical waveforms with the current measured at the channel base, all signals have been corrected for propagation delays. The current signal has been shifted backward in time to compensate for the transit time between the measuring shunt (at the ground-launcher) and the DSO through the ICLRT fiber optic network.   The radiometer signals were also shifted backward in time to compensate for the time required for light to propagate the horizontal distance, D, between the RTL launcher and the radiometers. Aligning the signals in this way facilitates a better understanding of the relationship between the measured current and optical waveforms.

Examples of the emissions produced by three RTL return strokes are shown in Figs 5-7 together with currents measured at the channel base.   In these figures, each stroke is shown on a five panel display. The horizontal axis on all panels gives the number of microseconds that have elapsed since the time of the RS onset ($t = 0$).   The top and widest panel shows the spectrally averaged irradiance waveforms in each optical band on an absolute scale. The left-center panel shows a shorter time-interval during the RS onset (excluding the LWIR signal because of its limited bandwidth), and the right-center panel shows the onset interval on a faster time-scale where the amplitudes have all been normalized to their peak values.   The bottom-left panel shows all signals near the RS onset with normalized amplitudes, and the bottom-right panel shows an interval near the end of the current using normalized amplitudes. The normalized panels have been included

to illustrate better the detailed time-relationships between the various signals.   In each panel, the current at the channel base is shown in black using a scale given on the right axis, and the scales for $\overline{L_\lambda}$ are on the left axis (note: all LWIR signals in this figure have all been multiplied by a factor of 10^3 relative to the other waveforms).   In all figures, the UV signal is blue, the VNIR signal is green, and the LWIR signal is red.
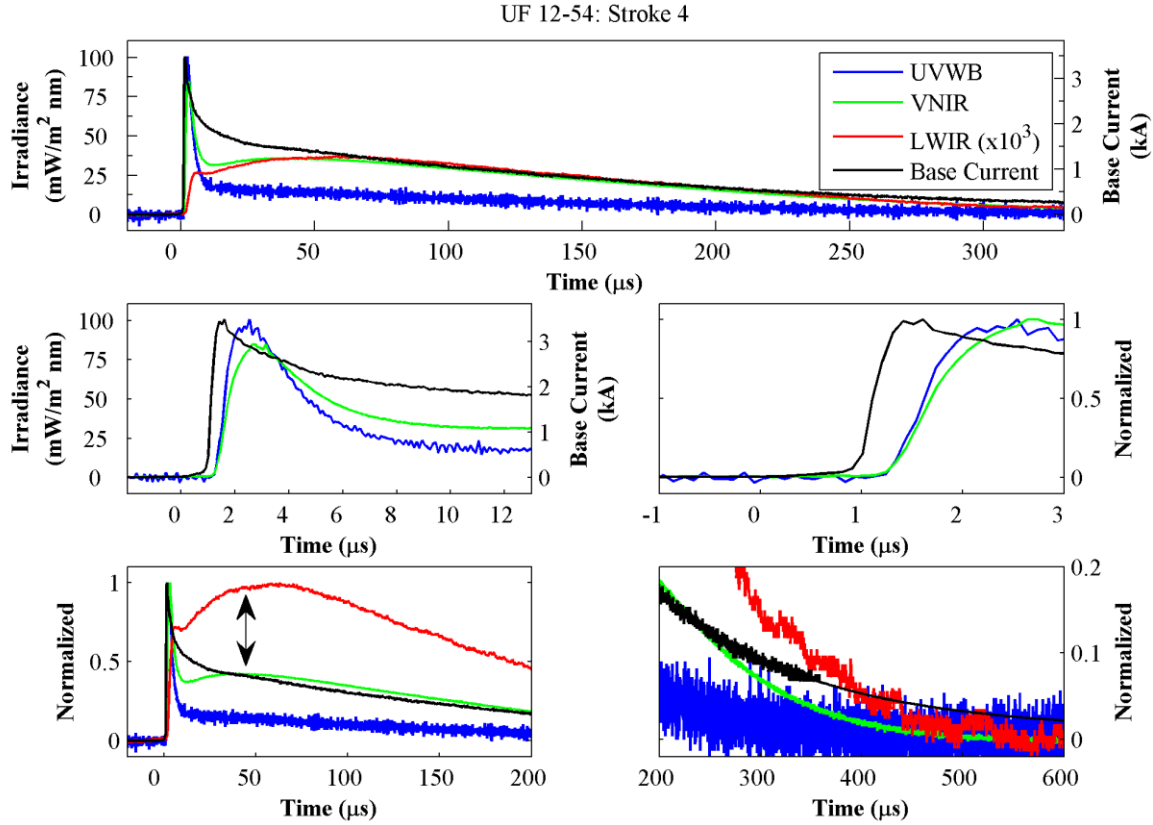

Figure 5: An example of the spectrally averaged irradiance ($\overline{L_\lambda}$) waveforms together with current measured at the channel base (black).   The $\overline{L_\lambda}$ waveforms use the scale shown on the left vertical axis, the current is on the right axis, and all LWIR waveforms have been multiplied by a factor of 10^3 to allow a better comparison on this scale.   The UV signal is blue, the VNIR signal is green, and the LWIR signal is red.   A secondary maximum (SM) in the VNIR is marked by a double arrow in the bottom-left panel.   Time $t = 0$ in this figure occurs 155.2462 ms after the data acquisition trigger time in UF 12-54.

Fig. 5 shows the fourth return stroke in RTL event UF 12-54. This event was a five stroke flash that was initiated on August 20, 2012, when the triggering rocket was approximately 220 m above ground. The fourth stroke was initiated by a dart-stepped leader; it had a relatively small peak current ($I_P = $ -3.5 kA); and the 10-90% current risetime was 0.4 µs. The UV and VNIR waveforms exhibit a fast rise to peak after the onset of the current, and this increase is likely dominated by the geometrical growth of the channel in the FOV of the sensor. After the initial peak, the VNIR and LWIR waveforms have a shoulder or secondary maximum (SM) that is marked by an arrow in the bottom-left panel, and it should be noted that this feature occurs while there is a steady decrease in the current. A SM is not present in the UV waveform. The 10-90%

risetimes of the UV and VNIR waveforms are 0.7 µs and 1.0 µs, respectively, and these signals peak 0.7 µs and 0.8 µs after I_P, respectively.   The LWIR waveform in Fig. 5 begins with a fast and likely band-limited rise that is due to the geometrical growth of the channel in the FOV, and then a slower and larger peak appears 60 µs after I_P. It is interesting to note that the peak LWIR signal occurs at approximately the same time as the SM in the VNIR.
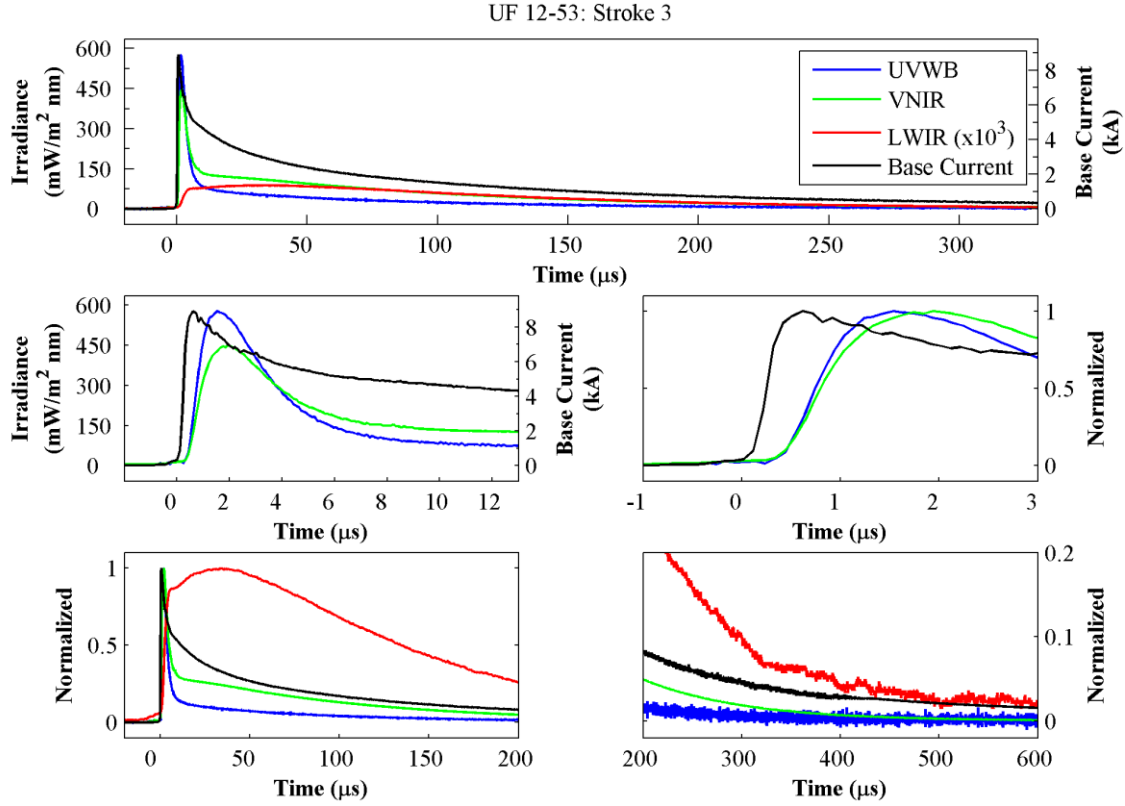

Figure 6:   See Fig. 5 for a description. $t = 0$ in this figure corresponds to 310.9791 ms after the data acquisition trigger in UF 12-53.

Fig. 6 shows the third stroke of RTL event UF 12-53. This event was a five stroke flash that was initiated on August 20, 2012 when the rocket was approximately 245 m above ground. This stroke was preceded by a normal dart leader; it had an I_P of -8.9 kA; and the 10-90% current risetime was 0.3 µs.   Again the UV emission rises faster and peaks earlier than the VNIR signal, and it has a larger peak spectral amplitude. The 10-90% risetimes of the UV and VNIR emissions are 0.7 and 0.9 µs, respectively, and the delays between I_P and the UV and VNIR peaks are 0.9 and 1.3 µs, respectively.   The LWIR waveform begins with a rapid increase, then there is a plateau that is followed by a more gradual rise to a peak that is broader in time than the UV and VNIR emissions. The peak LWIR emission occurs 33 µs after I_P.

Fig. 7 shows the eighth stroke of RTL event UF 12-35. This was a 13 stroke flash that was initiated on July 30, 2012 when the triggering rocket was about 300 m above the ground.   The stroke was preceded by a 'chaotic' dart leader; it had a relatively large I_P = -15.7 kA; and the 10-90 % current risetime was 0.2 µs. The optical waveforms have features that are similar to the previous examples, i.e. a fast rise to peak in the UV and VNIR followed by a fast decay relative to the current.   The UV and VNIR risetimes are 0.5 and 0.6 µs, respectively, and these emissions peak 0.6 and 0.8 µs after I_P.   The UV irradiance in Fig. 7 has a larger peak and faster decay than the VNIR, and the VNIR is broader in time.   The shape of the LWIR emission is similar to the previous examples, except there is not a distinct plateau after the FOV has been filled. The peak in the LWIR occurs 45 µs after I_P.
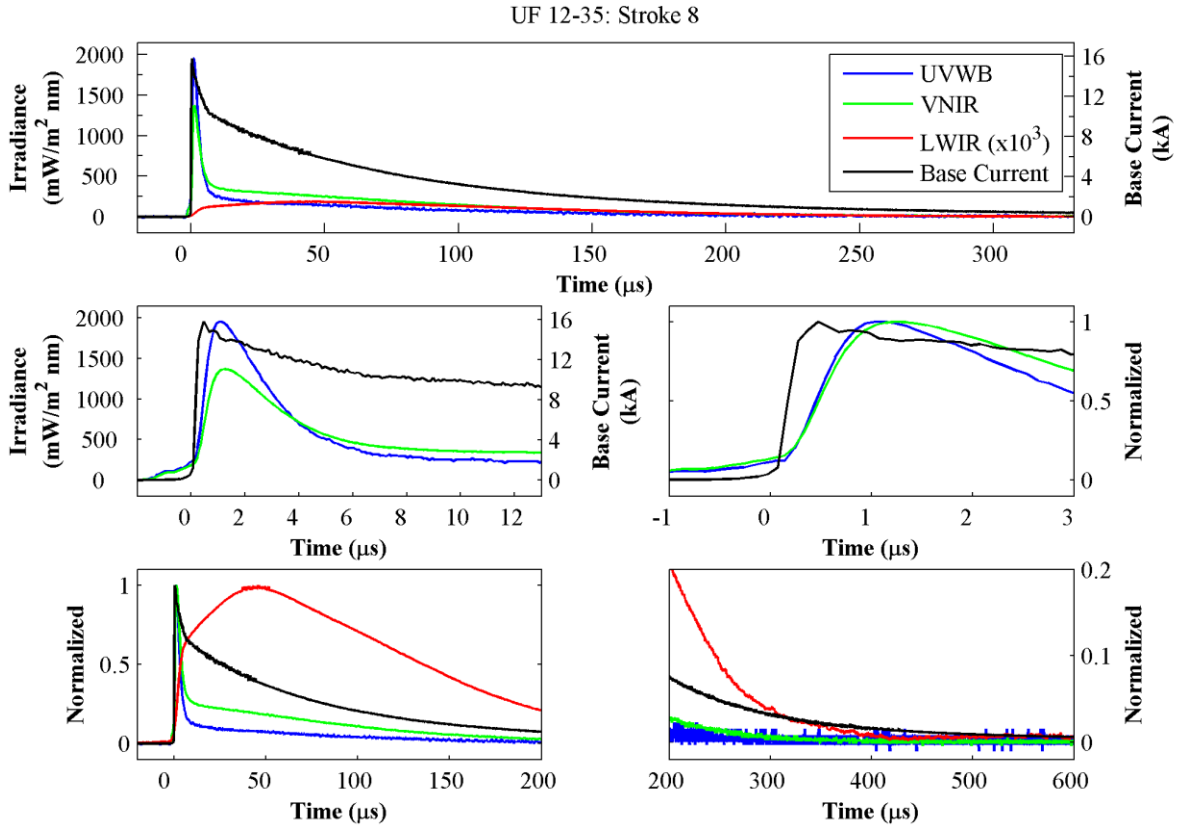

Figure 7:   See Fig. 5 caption for a description. t = 0 in this figure corresponds to 228.0200 ms after the data acquisition trigger in UF 12-35.

DISCUSSION

A total of 50 RS waveforms were suitable for detailed analysis, and all lowered negative charge to ground.   Table 1 lists the medians, means, and standard deviations of I_P together with our estimates of $\ell_{\lambda,\text{o}}$, and $\ell_{\lambda,\mathcal{R}}$ for the 50 strokes. Note here that the values of $\ell_{\lambda,\mathcal{R}}$ are larger than $\ell_{\lambda,\text{o}}$, a result that is expected because $\ell_{\lambda,\text{o}}$ represents a lower limit for the true peak power emitted at the source [*Quick et. al* 2014].   The median $\ell_{\lambda,\mathcal{R}}$ in the UV is about 45% larger than that median in the VNIR, and the median VNIR is

Table 1: Peak spectral power emitted by 50 RTL return strokes in 2012.

Spectral Band	I_p (kA)	$\ell_{\lambda,\mathrm{o}}$ (kW/nm-m)	$\ell_{\lambda\mathcal{R}}$ (kW/nm-m)
UV			
Mean ± Std	-12 ± 3.9	7.4 ± 4.8	10 ± 6.6
Median	-12	6.5	8.9
VNIR			
Mean ± Std	-12 ± 3.9	4.3 ± 2.6	7.0 ± 4.2
Median	-12	3.8	6.1
LWIR			
Mean ± Std	-12 ± 3.9	-	$(9.4 \pm 3.8) \times 10^{-4}$
Median	-12	-	9.4×10^{-4}

about 4 orders of magnitude larger than the LWIR median. The values of $\ell_{\lambda,\mathrm{o}}$ in the LWIR have not been included in Table 1 because the initial slopes of the LWIR signals were band-limited by the electronics rather than being due to the geometrical growth of the source in the FOV. It is important to note that the source power estimates in the UV and LWIR may be biased by the non-uniform responsivity of the detectors in those spectral bands as well as by the unknown spectral distribution of the source.

The onset of the optical waveforms that are produced by return strokes in RTL are the superposition of the geometrical growth of the channel in the FOV and also the temporal evolution of the source within the FOV. The signals from each of the three radiometers began with a fast, nearly linear rise and we assume that this feature corresponds to the rapid geometrical growth of the channel. We note in the examples shown in Figs. 5-7, that the onsets of the UV and VNIR occur simultaneously. The UV signal peaks before the VNIR, has a faster rising slope, and a shorter risetime. The LWIR waveform has a slower initial rise caused by the limited electronic bandwidth of that sensor, and the LWIR signal continues to rise toward a true peak after the FOV is completely filled. It is possible that the earliest portion of the LWIR signals are contaminated by a small leakage of shortwave radiation through the 8-12 μm passband filter, however at the time of the peak LWIR any contamination should be minimal. These results are qualitatively consistent with previous spectrally resolved observations such as *Krider* [1965] and *Orville* [1968a] who report that the short wavelength emissions from singly ionized atoms appear first in the lightning spectrum followed by a continuum and then line emissions from neutral atoms. We observe a similar transition here from short to long wavelengths as time progresses.

To gain an understanding of how the multiband energy distribution changes as a function of time we can examine the ratios of $\overline{L_\lambda}$ in the different spectral bands. Additionally, although it has been observed that the optically thin lightning channel emits a spectrally complex signature, it will be instructive to estimate an approximate source temperature by assuming the channel is a blackbody radiator and has an emission spectrum described by Plank's law. In this case, the $\overline{L_\lambda}$ ratios can be used to compute a source *color temperature*.

Fig. 8 shows two spectral ratios during the third RS of RTL event UF 12-53 (shown in Fig. 6) together with the inferred color temperatures starting at the time of the RS initiation. The left panel shows the UV

to VNIR or "short-wave" ratio over a 10 µs interval, and the right panel shows the VNIR to LWIR or "long-wave" ratio over a 600 µs interval. In the left panel the ratio is noisy prior to the RS onset which is likely due to the faint signal produced by the dart leader. After the RS onset there is a rapid rise in the short-wave ratio that peaks at 1.5 and corresponds to a color temperature of 7900 K at the time of the UV peak (0.7 µs). By 4 µs the ratio drops below 1.0 and then continues to decrease. This indicates that the
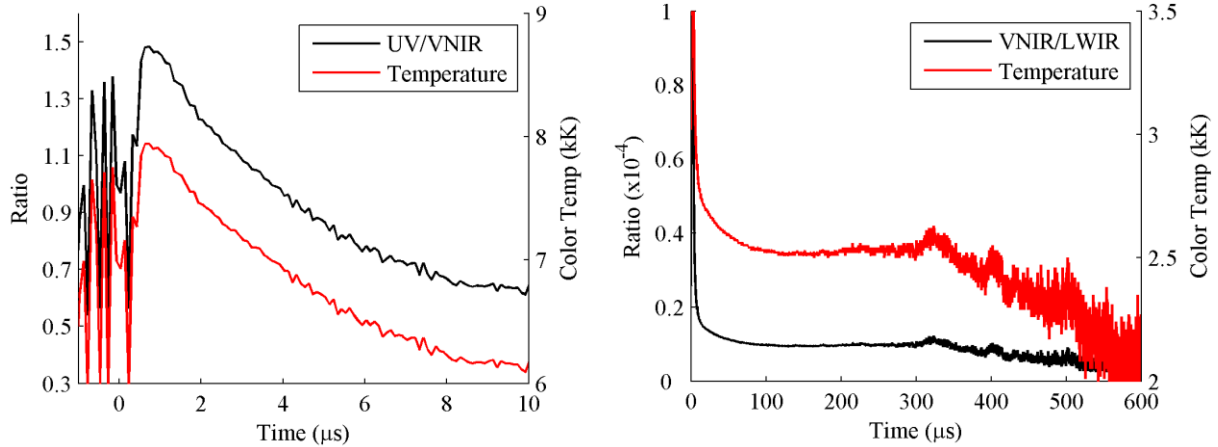

Figure 8: LEFT: The ratio of $\overline{L_\lambda}$ in the UV to $\overline{L_\lambda}$ in the VNIR band as a function of time for UF 12-53 stroke 3 (RS waveforms shown in Fig. 6) together with the color temperature of the source estimated from the ratio. Time $t = 0$ on the horizontal axis corresponds to the approximate time of the RS onset in the base current waveform taken to be 310.9791 ms as shown in Fig. 6. RIGHT: Same as left panel except with the ratio of VNIR to LWIR bands and the corresponding estimated temperature. Note the scale on the left axis indicates the magnitude of the ratio multiplied by 10^{-4}.

VNIR spectral band is radiating more power per nm than the UV at those times and the peak energy distribution is shifting from short to longer wavelengths. In the right panel there is a rapid decrease in the VNIR/LWIR ratio during the first few tens of µs followed by a plateau that corresponds to a color temperature of just over 2500 K. This plateau is sustained for more than 300 µs and is followed by a decrease in the ratio and temperature values. The decrease in the ratio corresponds to a change in the descending slope of the LWIR signal that can be seen in the lower right panel of Fig. 6 and may indicate an abrupt change in the thermodynamic and conductive properties of the channel.

A second example of the optical ratios and the corresponding color temperatures is given in Fig. 9 for the eighth RS of UF12-35 (shown previously in Fig. 7). The beginning temperature derived from the short-wave ratio indicates that the pre-RS channel was heated to a few thousand Kelvin by the chaotic-dart leader that preceded the RS. After initiation of the return stroke, the $\overline{L_\lambda}$ ratios rise rapidly in a way that is consistent with the short wavelength radiation increasing faster than the long wave. The UV to VNIR ratio peaks at 1.55 at the time of the UV peak (0.6 µs), and the color temperature is 8000 K. Following this maximum the UV to VNIR ratio drops to a value of 1.0 about 4 µs after onset, and then this ratio continues to decrease. The time evolution of the short-wave ratio in this stroke is very similar to the previous example even with the much larger I_P. The long-wave ratio indicates that the color temperature drops rapidly for the first few tens of µs and then plateaus between 2500 and 3000 K. At longer times the

amplitudes of the radiometer signals are comparable to the system noise so that the $\overline{L_\lambda}$ ratios become noisy, and we do not see the abrupt decrease in the long-wave ratio that was observed in the previous example.

All the color temperatures reported here are very likely too small. Previous studies based on time-and-space resolved slitless spectroscopy have found that the peak temperatures in return strokes are in the neighbourhood of 30,000 K and dart-leaders are reported to be close to 20,000 K [*Orville* 1968b, 1975]. Considering our incorrect approximation of the lightning channel as a blackbody radiator, and the non-uniform variations of the sensor spectral responsivities with wavelength, we expect an underestimate.
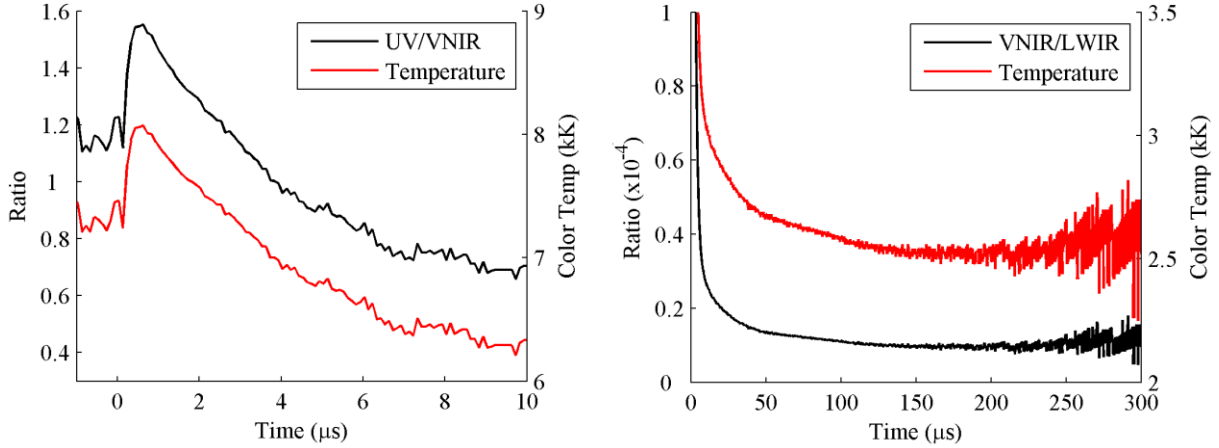

Figure 9: LEFT: The ratio of $\overline{L_\lambda}$ in the UV to $\overline{L_\lambda}$ in the VNIR band as a function of time for UF 12-35 stroke 8 (RS waveforms shown in Fig. 7) together with the color temperature of the source estimated from the ratio. Time $t = 0$ on the horizontal axis corresponds to the approximate time of the RS onset in the base current waveform taken to be 228.0200 ms as shown in Fig. 7. RIGHT: Same as left panel except with the ratio of VNIR to LWIR bands and the corresponding estimated temperature. Note the scale on the left axis indicates the magnitude of the ratio multiplied by 10^{-4}.

Quick and Krider [2013] have reported that the peak source power in the VNIR during natural lightning strokes is proportional to I_P^2. We find a similar relationship in the UV and VNIR measurements of RTL. Fig. 10 shows a plot of our estimates of $\ell_{\lambda,\mathcal{R}}$ verses I_P in all three spectral bands. The left panel shows a clear correlation between $\ell_{\lambda\mathcal{R}}$ and I_P^2 for the UV and VNIR datasets. The trend lines in the left panel are least squares fits of quadratic relationships constrained to pass through the origin and the determination coefficients are 0.81 and 0.87 for the UV and VNIR fits, respectively. The right panel shows a plot of the same variables in the LWIR, where there is clearly much more scatter and a lack of any real correlation between the quantities. This result expected because the LWIR peaks tens of μs after I_P, and the current and light in RTL become decoupled after the time of I_P [*Wang et al* 2005].
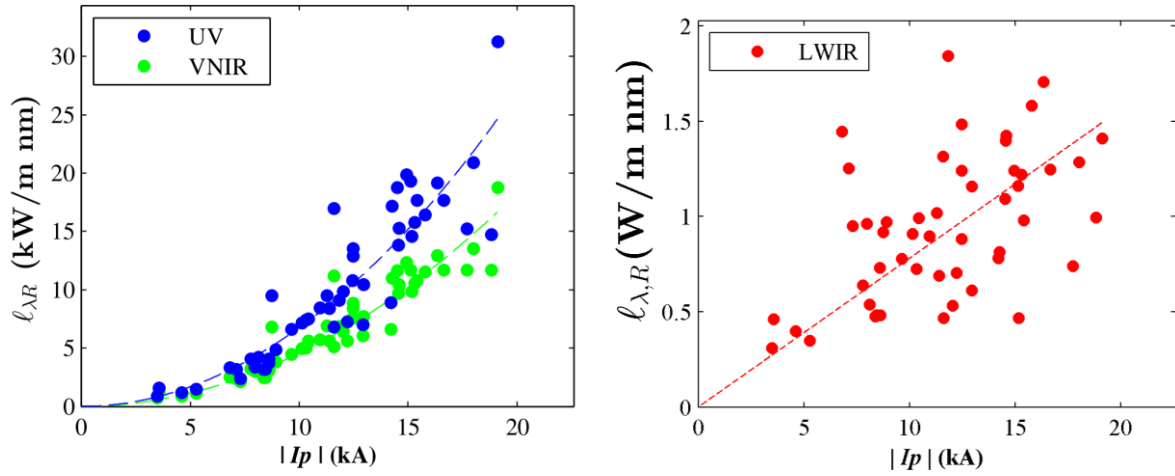
Figure 10: Left: $\ell_{\lambda\mathcal{R}}$ vs I_P for UV (blue) and VNIR (green). Both datasets are shown with a least squares quadratic fit line that is constrained to go through the origin. High correlation exists between I_P^2 and $\ell_{\lambda\mathcal{R}}$. The peak emission in the UV band has a higher proportionality to I_P^2 than the VNIR. Right: $\ell_{\lambda\mathcal{R}}$ vs I_P for LWIR. A least squares linear fit is shown for illustrative purposes. No significant correlation is observed between the two variables.

SUMMARY

By making calibrated multiband optical measurements of RTL we have found that the UV emissions rise faster and peak earlier than the VNIR emissions. Both spectral bands rise to peak in several tenths of a μs, and with the VNIR peaks 0.1 or 0.2 μs after the UV. Following a rapid rise during onset, the LWIR waveforms exhibit a slow rise to peak over an interval of 30-50 μs. Median estimates of the peak spectral power emitted per unit length are about 45% larger in the UV than in the VNIR, and the peak LWIR signal is about 4 orders of magnitude less than the UV and VNIR. An analysis of the spectral power in the UV and VNIR as a function of time shows that the UV emissions are initially the most intense, but the power shifts to the VNIR within a few μs, and then to the LWIR. Rough estimates of the color temperature of return stroke channels suggest peak temperatures that exceed 8000 K. Plots of the peak UV and VNIR spectral emissions show that the source power appears to be correlated with I_p^2.

ACKNOWLEDGMENTS

REFERENCES

Cummins, K. L., and M. J. Murphy (2009), An overview of lightning locating system: History, techniques, and data uses, with an in-depth look at the U.S. NLDN *IEEE Trans. EMC 51(3)*, 499-518.

Chen, M., T. Watanabe, N. Takagi, Y. Du, D. Wang, and X. Liu (2003), Simultaneous observations of optical and electrical signals in altitude-triggered negative lightning flashes, *J. Geophys. Res., 108*(D8), 4240. doi: 10.1029/2002JD002676

Gamerota, W. R., M. A. Uman, J. D. Hill, J. Pilkey, T. Ngin, D. M. Jordan, and C. T. Mata (2013), An "anomalous" triggered lightning flash in Florida, *J. Geophys. Res*., 118, 3,402-3,414, doi:10.1002/jgrd.50261

Guo, C. and E. P. Krider (1982), The optical and radiation field signatures produced by lightning return strokes, *J. Geophys. Res., 87*(C11), 8,913-8,922.

Guo, C., and E. P. Krider (1983), The optical power radiated by lightning return strokes, *J. Geophys. Res., 88*(C13), 8,621-8,622.

Hill, J. D., M. A. Uman, D. M. Jordan, J. R. Dwyer, H. Rassoul (2012), "Chaotic" dart leaders in triggered lightning: electric fields, x-rays, and source locations, *J. Geophys. Res.*, 117(D03118), doi: 10.1029/2011JD016737

Hill, J. D., J. Pilkey, M. A. Uman, D. M. Jordan, W. Rison, P. R. Krebhiel, M. I. Biggerstaff, P. Hyland, and R. Blakeslee (2013), Correlated lightning mapping array and radar observations of the initial stages of three sequentially triggered Florida lightning discharges, *J. Geophys. Res*., 118, 8,460-8,481, doi:10.1002/jgrd.50660

Idone, V. P., and R. E. Orville (1985), Correlated peak relative light intensity and peak current in triggered lightning subsequent return strokes, *J. Geophys. Res., 90*, 6,159-6164.

Jordan, D. M., V. P. Idone, V. A. Rakov, M. A. Uman, W. H. Beasley, and H. Jurenka (1992), Observed dart leader speed in natural and triggered lightning, *J. Geophys. Res.*, 97(D9), 9951-9957, doi: 10.1029/92JD00566

Krider, E. P., 1965; Time-resolved spectral emissions from individual return strokes in lightning discharges, *J. Geophys. Res.*, **70**, 2459-2460

Mach, D. M. and W. D. Rust (1989), Photoelectric return-stroke velocity and peak current estimates in natural and triggered lightning, *J. Geophys. Res., 94*(D11), 13,237-13,247.

Olsen III, R. C., D. M. Jordan, V. A. Rakov, M. A. Uman, and N. Grimes (2004), Observed one-dimensional return stroke propagation speeds in the bottom 170 m of a rocket-triggered lightning channel, *Geophys. Res. Lett., 31*, L16107, doi: 10.1029/2004GL020187.

Orville, R. E., 1968a ; A high-speed time-resolved spectroscopic study of the lightning return stroke : Part

I. a qualitative analysis, *J. Atmos. Sci.* **25**, 827-838.

Orville, Richard E., 1968b: A High-Speed Time-Resolved Spectroscopic Study of the Lightning Return Stroke: Part II. A Quantitative Analysis. *J. Atmos. Sci.*, **25**, 839–851.

Orville, Richard E., 1975: Spectrum of the Lightning Dart Leader. *J. Atmos. Sci.*, **32**, 1829–1837.   doi: http://dx.doi.org/10.1175/1520-0469(1975)032<1829:SOTLDL>2.0.CO;2

Pilkey, J. T., M. A. Uman, J. D. Hill, T. Ngin, W. R. Gamerota, D. M. Jordan, W. Rison, P. R. Krehbiel, H. E. Edens, M. I. Biggerstaff, and P. Hyland (2013), Rocket-and-wire triggered lightning in 2012 tropical storm Debby in the absence of natural lightning, *J. Geophys. Res.*, 118(13) 158-174, doi:10.1002/2013JD020501.

Qie, X., R. Jiang, C. Wang, J. Yang, J. Wang, and D. Liu (2011), Simultaneously measured current, luminosity, and electric field pulses in a rocket-triggered lightning flash, *J. Geophys. Res., 116*(D10102), doi: 10.1029/2010JD0135331

Quick, M. G. and E. P. Krider (2013), Optical power and energy radiated by natural lightning, *J. Geophys. Res., 118*, 1-12, doi: 10.1002/fgrd.50182.

Quick, M. G., E. P. Krider, K. L. Cummins, M. A. Uman, J. D. Hill, D. M. Jordan, W. R. Gamerota (2014), Optical Power and Energy Radiated by Return Strokes in Rocket-Triggered Lightning, *to be submitted to the J. of Geophys. Res.*

Schaal, M. M., J. R. Dwyer, Z. H. Saleh, H. K. Rassoul, J. D. Hill, D. M. Jordan, and M. A. Uman (2012), Spatial and energy distributions of X-ray emissions from leaders in natural and rocket triggered lightning, *J. Geophys. Res.*, 117(D15201), doi:10.1029/2012JD017897

Wang, D., V. A. Rakov, M. A. Uman, N. Takagi, T. Watanabe, D. E. Crawford, K. J. Rambo, G. H. Schnetzer, R. J. Fisher, Z.-I Kawasaki (1999a) Attachment process in rocket-triggered lightning strokes, *J. Geophys. Res.,* 104, D2 2143-2150

Wang, D., N. Takagi, and T. Watanabe (1999b), Observed leader and return-stroke propagation characteristics in the bottom 400 m of a rocket-triggered lightning channel, *J Geophys. Res., 104*(D12) 14,369-14,376.

Wang, D., N. Takagi, T. Watanabe, V. A. Rakov, M. A. Uman, K. J. Rambo, and M. V. Stapleton (2005), A comparison of channel-base currents and optical signals for rocket-triggered lightning strokes, *Atmos. Res., 76*, 412-422.

Wang, D., N. Takagi, W. R. Gamerota, M. A. Uman, J. D. Hill, D. M. Jordan (2013), Initiation process of return strokes in rocket-triggered lightning, *J. Geophys. Res.,* 118, 9880-9888, do1:10.1002/jgrd.50766

Wang, D., W. R. Gamerota, M. A. Uman, N. Takagi, J. D. Hill, J. Pilkey, T. Ngin, D. M. Jordan, S. Mallick, V. A. Rakov (2014), Lightning attachment process of an "anomalous" triggered lightning discharge, *J Geophys. Res.*, 119, doi:10.1002/2013JD020787

Winn, W. P., E. M. Eastvedt, J. J. Trueblood, K. B. Eack, H. E. Edens, G. D. Aulich, S. J. Hunyady, and W. C. Murray (2012), Luminous pulses during triggered lightning, *J. Geophys. Res. 117*(D10204), doi: 10.1029/2011JD017105.